Journal of Cosmology and Astroparticle Physics
An IOP and SISSA journal

Nonlinear resonance of Kolmogorov–Arnold–Moser tori in bouncing universes

H P de Oliveira[1], **I Damião Soares**[2] **and E V Tonini**[3]

[1] Instituto de Física—Universidade do Estado do Rio de Janeiro, CEP 20550-013 Rio de Janeiro, RJ, Brazil
[2] Centro Brasileiro de Pesquisas Físicas, Rua Dr Xavier Sigaud 150, Urca, Rio de Janeiro CEP 22290-180-RJ, Brazil
[3] Centro Federal de Educação Tecnológica do Espírito Santo, Avenida Vitória, 1729, Jucutuquara, Vitória CEP 29040-780-ES, Brazil
E-mail: oliveira@dft.if.uerj.br, ivano@cbpf.br and tonini@cefetes.br

Received 3 October 2005
Accepted 30 January 2006
Published 27 February 2006

Online at stacks.iop.org/JCAP/2006/i=02/a=015
doi:10.1088/1475-7516/2006/02/015

Abstract. The dynamics of closed Friedmann–Robertson–Walker (FRW) universes with a massive inflaton field is examined where Friedmann equations are corrected by the introduction of a potential term that implements non-singular bounces in the early evolution of the universe. This potential term arises from quantum gravity/high-energy corrections to cosmological scenarios near the singularity and is semiclassical in nature, being effective only when the scale factor is very small. For certain windows in the parameter space labelled by the scalar field mass and the conserved Hamiltonian, nonlinear resonance phenomena take place. Nonlinear resonance may induce the destruction of Kolmogorov–Arnold–Moser (KAM) tori that trap the inflaton, leading to a rapid growth of the scale factor and the scalar field, with disruption of metastable states and consequent escape of the universe into inflation. We make a numerical/analytical approach to the nonlinear resonance phenomena, characterizing a particular resonance by its characteristic periodic orbits and by the structure of the associated diffusion pattern. The diffusion occurs when the orbit escapes through a Cantorus in the border of primary KAM islands that encloses the characteristic periodic orbits of the resonance. The windows of parametric resonance, characterized by an integer $n \geq 2$ (associated with the ratio of the frequencies in the scale factor/scalar field degrees of freedom) are the ones that strongly favour inflation in the system.

1475-7516/06/02015+24$30.00

JCAP02(2006)015

We discuss how generic this behaviour is for inflationary models, and its possible consequences for structure formation.

Keywords: inflation, physics of the early universe

Contents

1. Introduction

The initial conditions of our present expanding universe must have been fixed when the early universe emerged from the semiclassical Planckian regime and started its classical evolution. From these initial conditions the universe starts its evolution with the dynamics ruled by Einstein's field equations. Backwards evolution of the initial conditions using classical equations of motion drives the system towards a neighbourhood of a singular point, where the classical regime is no longer valid and must be substituted by the quantum regime. Quantum gravity corrections to cosmological scenarios near the singularity have been the object of much recent research, from loop quantum cosmology [1] to string theory [2], all of them leading to the presence of bounces in the scale factor of the model. On the other hand, the existence of infinitely bouncing universes in the realm of closed Friedmann–Robertson–Walker (FRW) universes endowed with a simple form of massive scalar field has a long history [3]. These structures have received considerable attention in connection with the study of chaotic dynamics in the early universe [4]. Also, the study of closed cosmological models has the further advantage that they are more adapted for the development of the quantum approach to the origin of the universe. Furthermore, bouncing universes resulting as a consequence of corrections of the field equations due to quantum gravity effects are considered seriously as non-singular models compatible with observational data [5]. Recently, an interesting possibility for such cosmologies has been described in brane-world model scenarios for which corrections to Friedmann equations on the brane due to the influence of a bulk geometry allow us to produce non-singular bounces in the scale factor [6]. These corrections effectively result in a repulsive force that avoids the singularity, and are dominant in its neighbourhood. In the realm of the above-discussed quantum corrections near the cosmological singularity, we are then led to consider the introduction of an extra potential term in Friedmann's equations when

JCAP02(2006)015

treating a class of FRW models with a conformally coupled massive scalar field ϕ (the inflaton field) plus a perfect fluid. For perfect fluid cosmologies this correction term may be assumed to be of the form $-A/a^{\alpha}$, where A is a positive constant, a is the scale factor and the integer $\alpha \geq 2$. For simplicity in performing a numerical/analytical analysis of the dynamics we will fix $\alpha = 6$ in the present paper, but the features of the dynamics may be substantially different for other choices of α and deserve future examination[4]. This choice was also considered in models with radiation and a phantom fluid with an equation of state $p = \rho \propto a^{-6}$ [7]. For the conformally coupled scalar field we assume the potential $U(\phi) = \Lambda + m^2\phi^2/2$ where the cosmological constant term Λ is considered to correspond to the vacuum energy of the inflaton field and ϕ its spatially homogeneous expectation values. We further assume that the model contains a perfect fluid describing radiation ($p = \rho/3$).

Throughout this paper we use units such that $\hbar = c = 1$ and $8\pi G = 1$.

We start from the line element of a closed FRW model

$$\mathrm{d}s^2 = N(t)^2\,\mathrm{d}t^2 - a(t)^2\left[\frac{\mathrm{d}r^2}{1-kr^2} + r^2(\mathrm{d}\theta^2 + \sin^2\theta\,\mathrm{d}\phi^2)\right] \tag{1}$$

where $a(t)$ is the scale factor and $N(t)$ is the lapse function. The Lagrangian density of the model is given by

$$\mathcal{L} = \mathcal{L}_{\mathcal{G}} + \mathcal{L}_{\phi} + \mathcal{L}_{\mathcal{I}} + \mathcal{L}_{\rho} \tag{2}$$

where $\mathcal{L}_{\mathcal{G}} = -\sqrt{-g}\ R/2$ is the Lagrangian density of the gravitational field (1), $\mathcal{L}_{\phi} = \sqrt{-g}(\phi^{,\mu}\phi_{,\mu}/2 - U(\phi))$ is the Lagrangian density of the inflaton (scalar) field and $\mathcal{L}_{\rho} = -\sqrt{-g}\ \rho$ is the Lagrangian density of the perfect fluid content. The term

$$\mathcal{L}_{\mathcal{I}} = \sqrt{-g}(\xi\phi^2 R/2) \tag{3}$$

describes the non-minimal coupling of the inflaton with gravitation and is partly motivated by quantum calculations in curved spacetimes (taking into account quantum backreaction, renormalization, string theory, etc) and partly by the possibility of constructing successful inflationary and pre-inflationary scenarios [8]. The case $\xi = 0$ is the usual minimal coupling of the scalar field with gravitation, and $\xi = 1/6$ is the so-called conformal coupling [9].

In the above, g is the determinant of the metric (1) and R is the Ricci scalar given by

$$R = -\frac{6}{N^2}\left(\frac{\ddot{a}}{a} + \frac{\dot{a}^2}{a^2} + N^2\frac{k}{a^2} - \frac{\dot{a}\dot{N}}{aN}\right). \tag{4}$$

Due to the spatial homogeneity of the model, the total action can then be expressed as

$$S = V_0\int \mathrm{d}t\ Na^3\left[-\frac{R}{2}(1-\xi\phi^2) + \frac{1}{2N^2}\dot{\phi}^2 - U(\phi) - \rho\right] \tag{5}$$

where the constant V_0 stands for the volume of the spatial sections $t =$ constant (which have the topology of S^3, or S^3 factorized by a discrete group of identifications [10]).

[4] We note that the choice $n = 6$ corresponds to bulk–brane corrections in Friedmann's equations with dust.

Discarding the total time derivative term in the integrand of (5), and further introducing a new scalar field variable φ such that $\phi = \varphi a^n$, where

$$n + 6\xi = 0, \tag{6}$$

equation (5) turns into

$$S = V_0 \int \mathrm{d}t \left[-\frac{3a\dot{a}^2}{N} + 3kaN + \frac{a^{(3-12\xi)}}{2N}\dot{\varphi}^2 + \frac{3\xi(1-6\xi)}{N}\dot{a}^2 a^{(1-12\xi)}\varphi^2 - 3kaN\xi\varphi^2 \right.$$
$$\left. - Na^3 U(\varphi a^{-6\xi}) - 3k\xi N\varphi^2 a^{(1-12\xi)} - Na^3\rho \right]. \tag{7}$$

For matters of simplification, by a proper rescaling of the scale factor and the r coordinate we set $V_0 = 1$ and $k = 1$ in what follows. From the kinetic terms of (7) we define the momenta canonically conjugate to a and φ, respectively, as

$$p_a = -\frac{6a\dot{a}}{N} + \frac{6\xi(1-6\xi)}{N}\ \dot{a}\ \varphi^2 a^{(1-12\xi)}$$
$$p_\varphi = \frac{a^{(3-12\xi)}}{N}\ \dot{\varphi}$$

so that (7) assumes the canonical form

$$S = \int \mathrm{d}t\ \ (\dot{a}p_a + \dot{\varphi}p_\varphi - NH) \tag{8}$$

where

$$H = \frac{p_a^2}{12a[-1 + (1-6\xi)\xi\varphi^2 a^{-12\xi}]} + \frac{p_\varphi^2}{2a^{(3-12\xi)}} - 3a + a^3 U(\varphi a^{-6\xi}) + 3\xi\varphi^2 a^{(1-12\xi)} + a^3\rho. \tag{9}$$

Extremizing the action (8) with respect to variations in N results in the Hamiltonian constraint

$$H = \frac{p_a^2}{12a[-1 + (1-6\xi)\xi\varphi^2 a^{-12\xi}]} + \frac{p_\varphi^2}{2a^{(3-12\xi)}}$$
$$- 3a + a^3 U(\varphi a^{-6\xi}) + 3\xi\varphi^2 a^{(1-12\xi)} + a^3\rho = 0. \tag{10}$$

Partly for reasons of analytical simplicity in the analysis of nonlinear resonance phenomena, in the remainder of the paper we will restrict ourselves to the dynamics in the conformal coupling case $\xi = 1/6$. The dynamics in the minimal coupling case $\xi = 0$ will present analogous features and will not be discussed here. For an extended range of values of ξ, a larger parameter space analysis is demanded and will be the object of a future investigation. As discussed previously, the fluid content of the model is given by

$$\rho = E_0 a^{-4} - Aa^{-6} \tag{11}$$

where E_0 is a constant of motion proportional to the total energy of the radiation fluid and the second term is the correction term arising from the bulk geometry. In the conformal time gauge $N = a$, the dynamics of the model may then be derived from the Hamiltonian constraint expressed in the form

$$H = -\tfrac{1}{2}(p_\varphi^2 + \varphi^2) + \tfrac{1}{12}p_a^2 + V(a) - \tfrac{1}{2}m^2 a^2\varphi^2 - E_0 = 0. \tag{12}$$

JCAP02(2006)015

In the above $V(a)$ is a potential in the gravitational sector given by

$$V(a) = 3a^2 - \Lambda a^4 + \frac{A}{a^2}, \tag{13}$$

where can be found, respectively, the contributions of the curvature term, the cosmological constant and the correction term arising from the bulk geometry (the latter responsible for the bounces).

For the sake of completeness it will be useful to give a more detailed explanation of the basic structure of the phase space of the model. We note first that the Hamiltonian (12) is separable for $m^2 = 0$, that the mass term couples the two degrees of freedom making the system non-integrable. The critical points, or equivalently the stationary solutions of the Hamiltonian equations derived from (12) basically constitute the skeleton of the phase space under consideration, and therefore will be crucial to our study. It can be shown that the critical points are characterized by

$$p_a = p_\varphi = 0, \qquad \varphi = 0, \qquad V'(a) = 0, \tag{14}$$

namely, they are connected to the extrema of the potential $V(a)$. For positive values of A and Λ and in the region $a \geq 0$ there are only two critical points, P_0 and P_1, associated with the maximum and minimum of the potential, respectively. P_0 corresponds to the configuration of the Einstein static universe with an energy content having a contribution from the quantum potential, while the critical point P_1 is a stable static solution, arising from the dynamical balance between the energy content of the radiation fluid and the negative energy density connected to the quantum potential. It is worth remarking that P_0 is a saddle-centre and P_1 a pure centre, as can be seen from the linearization of the dynamics about each critical point [11]. Both critical points are contained in a two-dimensional submanifold of the phase space, denoted the invariant plane and defined by

$$\varphi = 0, \qquad p_\varphi = 0, \tag{15}$$

where the dynamics is integrable. Orbits with initial conditions on this plane are totally contained in it, actually corresponding to the dynamics in the sector (a, p_a) of the separable case $m = 0$. The phase portrait in the invariant plane is depicted in figure 1(b), and is connected to the one-dimensional motion in the potential $V(a)$. We remark that due to the character of fluctuations of φ, physical configurations will correspond to initial conditions near the invariant plane.

Also, a straightforward analysis of the infinity of phase space shows the presence of a pair of critical points in this region, one acting as an *attractor* (stable de Sitter configuration) and the other as a *repeller* (unstable de Sitter configuration). The scale factor approaches the de Sitter attractor as $a(\tau) \sim (C_0 - \tau)^{-1}$ for $\tau \to C_0$, where τ is the conformal time (or as $a(t) \sim \exp(t\sqrt{\Lambda/3})$ for $t \to \infty$, where t is the cosmic time).

It is worth noticing from figure 1 that the critical point P_0, connected to the maximum of the potential, is engendered by the positive cosmological constant. Combined with the barrier generated by the quantum correction it allows for the presence of perpetually bouncing universes in the invariant plane figure 1(b). If the cosmological constant decreases to zero the domain of phase space available for these bouncing solutions decreases, and in the limit $\Lambda = 0$ only solutions with one single bounce are possible. They have an analogous behaviour with the integrable solutions shown in the phase portrait of

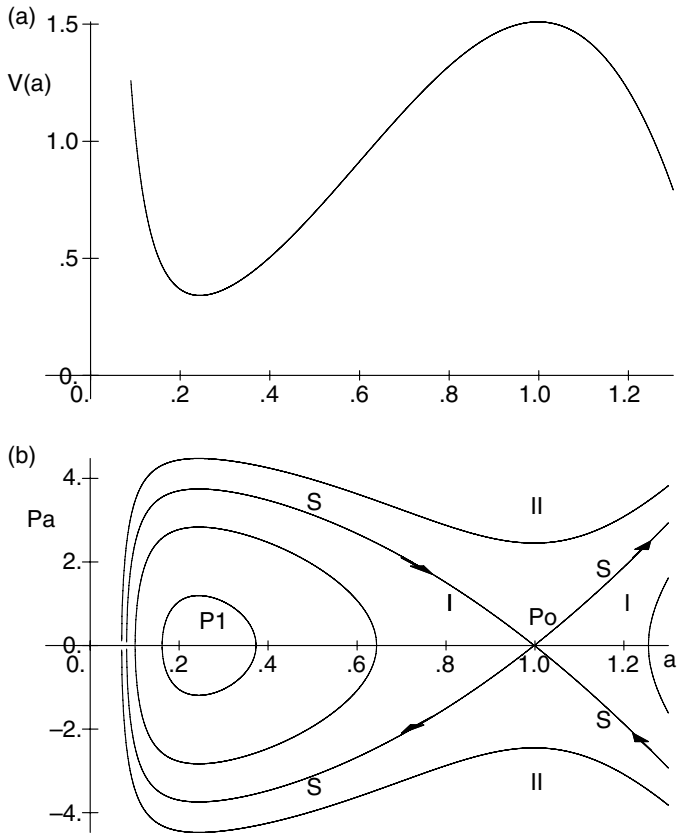

Figure 1. (a) Plot of the potential $V(a)$ for positive Λ and A. (b) The phase portrait of the invariant plane with the critical points P_0 and P_1. The separatrices S are asymptotic orbits to the saddle-centre P_0.

figure 1(b) for $E_0 > E_{P_0}$, where E_{P_0} is the value of the energy constant for the saddle-centre P_0. The purpose of the present paper is to treat dynamical configurations with initial conditions for which the universe undergoes a series of bounces before the universe enters an inflationary regime. Indeed, these configurations represent a hypothetical pre-inflationary phase where the influence of the terms arising from quantum gravity corrections plays the fundamental role in preventing the initial singularity, and producing a non-trivial dynamics before the exit to inflation. This exit to inflation occurs whenever a given orbit asymptotically approaches the de Sitter configuration. The inflationary phase is characterized by the de Sitter configuration driven by the cosmological constant understood as the vacuum energy of the scalar field that is dominant during inflation. In this scenario, the model envisaged describes a pre-inflationary phase for which the escape to inflation is represented by the asymptotic approach to the de Sitter solution. For this reason the vacuum energy Λ is actually what drives the universe to inflation whereas the term $m^2\phi^2/2$ describes the effect of small fluctuations of the inflaton field about its vacuum state.

The constant of motion E_0 corresponds to a bounded motion in the integrable case $m = 0$, and to initially bounded motion in the non-integrable cases when stable configurations may be disrupted by nonlinear resonance phenomena. Windows of

resonance in the parameter space, labelled by the mass of the inflaton m and the constant of motion E_0, favour inflation since the resonances destroy the Kolmogorov–Arnold–Moser (KAM) tori that trap the inflaton about the origin ($\varphi = 0, p_\varphi = 0$). The nonlinear resonance of KAM tori produces complex dynamical phenomena, such as long-time diffusion through Cantori, that will also be object of the present paper since they favour inflation after a process of long-time diffusion.

We organize the paper as follows. In section 2 we make a numerical construction of the resonance chart of the system to localize the windows of resonance, and develop an analytical treatment that allows us to label the resonances with an integer $n \geq 2$. The action-angle variables introduced will be useful in the interpretation of numerical results of the remaining sections. In sections 3 and 4 we examine dynamical patterns near odd and even resonances, including the structure of bifurcated periodic orbits, characteristic of the resonance, as well as the presence of Cantori and stochastic webs in phase space through which a long-time diffusion of orbits takes place with final escape to the de Sitter attractor at infinity. In section 5 the diffusion of orbits is examined, and comparison and distinction of the dynamical behaviour of initial physical conditions for inflation is made, whether the system is in a resonance window or in a parametric stability region. Finally in section 6 we discuss how generic the resonance phenomena are in inflationary models and their possible consequences for structure formation.

2. Analytical approach to the resonance chart of the system

Let us consider the dynamics in the energy surface E_0 corresponding to bounded motion in the integrable case $m = 0$, or to initially bounded motion in the non-integrable cases. This phase-space region can indeed be characterized as a nonlinear neighbourhood of the centre P_1. The results of the present section rely heavily on the analytical treatment leading to an accurate and useful form of the Hamiltonian in action-angle variables to be introduced below.

We start from the integrable case $m = 0$ in which the motion is separable with the separately conserved quantities $E_a = p_a^2/12 + V(a)$ and $E_\varphi = (p_\varphi^2 + \varphi^2)/2$, satisfying $E_0 = -E_\varphi + E_a$. For $E_a < V(P_0)$ the periodic orbits of the sector (a, p_a), associated with $E_a = \text{const.}$, are analytically expressed as

$$a^2(\tau) = a_3^2 + (a_2^2 - a_3^2)\mathrm{sn}^2\left(\frac{\sqrt{3\Lambda(a_1^2 - a_3^2)}}{3}\tau \mid \mu\right), \tag{16}$$

where $a_3 < a_2 < a_1$ are the three real positive roots of the function $V(a) - E_a = 0$, and $\mu = (a_2^2 - a_3^2)/(a_1^2 - a_3^2)$ is the modulus of the Jacobian elliptic sine, with corresponding frequency

$$\nu_a = \frac{\sqrt{3\Lambda(a_1^2 - a_3^2)}}{6K(\mu)}, \tag{17}$$

where $K(\mu) = (\pi/2)F(\frac{1}{2}, \frac{1}{2}; 1; \mu)$ is the complete elliptic integral of the first kind, with $F(\frac{1}{2}, \frac{1}{2}, 1; \mu)$ denoting the hypergeometric function [12]. The two tori of the integrable case are the topological product of the above class of periodic orbits parametrized by E_a with the periodic orbits of the harmonic oscillator parametrized by E_φ with frequency $\nu_\varphi = 1/2\pi$.

For a small coupling parameter m the KAM theorem [13] establishes the stability of tori with a sufficiently incommensurate frequency ratio, that in the present case means sufficiently irrational ν_a.[5] Other integrable tori are destroyed by the non-integrable perturbation, and the region between two remaining invariant tori presents an intricate dynamics [14]. However, this dynamics is bounded by the two invariant tori with irrational ν_a implying in a certain sense the stability of the dynamics. The importance of KAM tori for Hamiltonian systems with two degrees of freedom comes from the fact that they prevent the diffusion of trajectories in the whole phase space, and thus prevent, in our model, an escape to inflation. However, when m increases, that is when the non-integrability of the system increases, numerical experiments show that more and more invariant tori are destroyed [15] and the breakup of KAM tori may lead to a loss of stability of the system. An important mechanism for this breakup is the nonlinear resonance of tori.

For future reference, we note that the periodic orbits of the sector (a, p_a), in the integrable case, will be represented by the centre (elliptic fixed point) $(\varphi = 0, p_\varphi = 0)$ in the Poincaré map with surface of section $p_a = 0$. For small m this picture is maintained with $(\varphi = 0, p_\varphi = 0)$ as a centre of a primary KAM island. Let us now examine what happens to other regions of the parameter space (E_0, m) of the system.

We start by expressing the dynamical equations derived from the Hamiltonian constraint (12) as

$$\ddot{a} + \tfrac{1}{6}[V'(a) - m^2 a\varphi^2] = 0, \tag{18}$$

$$\ddot{\varphi} + (1 + m^2 a^2)\varphi = 0. \tag{19}$$

If now m is small and/or we start from an initial condition $\varphi = \varphi_0$ also small (for instance, near the invariant plane), we can neglect the term proportional to m in equation (18) and the motion in the degree of freedom φ is approximately described by the Lamé equation

$$\ddot{\varphi} + \left[1 + m^2\left(a_3^2 + (a_2^2 - a_3^2)\mathrm{sn}^2\left(\tfrac{1}{3}\sqrt{3\Lambda(a_1^2 - a_3^2)}\tau \mid \mu\right)\right)\right]\varphi = 0. \tag{20}$$

Parametric resonance occurs when the ratio

$$R = \frac{\nu_a}{\tilde{\nu}_\varphi}, \tag{21}$$

is a rational number, where ν_a is given in (17) and[6]

$$\tilde{\nu}_\varphi = \frac{1}{2\pi}\sqrt{1 + \frac{m^2}{2}\left[a_2^2 + a_3^2 + \frac{\mu^2}{4}(a_1^2 - a_3^2)\right]}. \tag{22}$$

Under this condition φ begins to grow exponentially in time and to act on the dynamics of the scale factor a, which in turn will modify equation (20). This feedback will restructure the resonance, either (i) leading the dynamics into a more unstable behaviour, with

[5] By sufficiently irrational, we mean a number α that is badly approximated by any rational number n/m, namely, it satisfies the inequality $|\alpha - n/m| \geq c/m^{(2+\epsilon)}$ for positive constants c, ϵ (see [14]).

[6] It is worth noting that, for values of $m \geq 14$ and $E_0 \leq 1.0$, we can improve the approximation for the instability zones of the exact dynamics by correcting $\tilde{\nu}_\varphi$ in equation (22) to $\tilde{\nu}_\varphi = (1/2\pi)\sqrt{1 + (m^2/2)(a_2^2 + a_3^2)}$.

amplification of the resonance mechanism and consequent breaking of the KAM tori and escaping of the orbits; (ii) leading the orbits to a general chaotic motion in a bounded region of phase space confined between two KAM tori; or (iii) when the parameters of the model are in the neighbourhood of a resonance island, leading to diffusion through Cantori and stochastic webs, with a final exit to inflation. These general nonlinear resonance mechanisms can be given an approximate analytical treatment, through which we can fix the dominant resonances in the system, namely, the rational numbers R in (21) which will correspond to the dominant resonances. This treatment, made along the lines of [15], will allow us to establish numerically domains of the parameter space and initial conditions for the full Hamiltonian dynamics of (12), where nonlinear resonance occurs and is able to enhance the escape of orbits into the inflationary regime.

Let us approximate the Hamiltonian (12) by substituting in the non-integrability term $m^2a^2\varphi^2/2$ the variable a by its solution (16), and afterwards introduce suitable action-angle variables $(\mathcal{J}_a, \Theta_a, \mathcal{J}_\varphi, \Theta_\varphi)$. The choice of variables was dictated by the approximation considered, which represents a further step beyond the analysis of parametric resonances in the linear regime of equation (20).

For the sector (a, p_a) we define the canonical conjugate variables $\mathcal{J}_a$ and Θ_a by

$$\begin{aligned} \mathcal{J}_a &= \oint p_a \, \mathrm{d}a = 4\sqrt{3}\int_{a_3}^{a_2} \sqrt{E_a - V(a)}\, \mathrm{d}a, \\ \Theta_a &= \nu_a \tau, \end{aligned} \tag{23}$$

and in the sector (φ, p_φ) the variables $\mathcal{J}_\varphi$ and Θ_φ defined by the canonical transformations

$$\begin{aligned} \varphi &= \sqrt{\frac{\mathcal{J}_\varphi}{2\pi^2\tilde{\nu}_\varphi}}\ \sin(2\pi\Theta_\varphi), \\ p_\varphi &= \sqrt{2\mathcal{J}_\varphi\tilde{\nu}_\varphi}\ \cos(2\pi\Theta_\varphi). \end{aligned} \tag{24}$$

In the above equations $\nu_a \equiv (\partial E_a/\partial \mathcal{J}_a)$ (see equation (17)) and we define the angle variable $\Theta_\varphi = \tilde{\nu}_\varphi \tau$ such that both Θ_a and Θ_φ vary in the interval $[0, 1]$ during a complete cycle of the original variables. We remark that in the numerical experiments considered in the remainder of the paper we have $E_a \simeq E_0$ in the initial stage of the dynamics. However, E_a is not conserved as the dynamics proceeds, the interaction term being responsible for the exchange of energy with the sector E_φ.

In the action-angle variables defined above the approximate Hamiltonian can be conveniently expressed as

$$H = E_a(\mathcal{J}_a) - \mathcal{J}_\varphi\tilde{\nu}_\varphi - \frac{m^2\mathcal{J}_\varphi}{4\pi^2\tilde{\nu}_\varphi}(a_2^2 - a_3^2)\left[\frac{1 - cn(2u)}{1 + \mathrm{d}n(2u)} - \frac{1}{2}\right]\sin^2(2\pi\Theta_\varphi), \tag{25}$$

where the argument in the Jacobian elliptic functions is $u \equiv 2K(\mu)\Theta_a$. Taking into account that $\mu < 1$ and using the expansion of the elliptic functions in terms of circular functions with argument $v = \pi u/(2K(\mu))$, equation (25) results in yields

$$H = E_a(\mathcal{J}_a) - \mathcal{J}_\varphi\tilde{\nu}_\varphi - m^2\mathcal{J}_\varphi\left[\sum_{n=1} B_n(\mu)\cos(2n\pi\Theta_a)\right]\cos(4\pi\Theta_\varphi), \tag{26}$$

where $B_n(\mu)$ are numerical coefficients depending on μ. As we will see in the numerical experiments made with the exact dynamics, the approximate expression equation (26) will be extremely efficient for localizing and classifying the resonances.

The parametric resonance condition for (21) obtained from the Lamé equation (20) is contained in the more accurate Hamiltonian (26), from which the nature of the resonances can now be qualitatively analysed. Indeed, from equation (26) we can obtain that in this instance the dominant resonances are the ones for which the ratio $R = \nu_a/\tilde{\nu}_\varphi = 2/n$, where n is an integer, $n \geq 2$. These numbers will fix the values of m and/or of E_0 of the parameter space, in the neighbourhood of which a resonance occurs. To see this let us integrate Hamilton's equations derived from (26) for a given term n of the series. To a first approximation we may take $J_\varphi = J_\varphi^{(0)} = \text{const}$ in the last term of the right-hand side of (26), and equal to its value in the integrable case. We then obtain

$$J_a \simeq \sum_n \frac{m^2 K_n(\mu)}{2\pi n \tilde{\nu}_\varphi} \left[\frac{\cos(2\pi n\Theta_a - 4\pi\Theta_\varphi)}{R - 2/n} + \frac{\cos(2\pi n\Theta_a + 4\pi\Theta_\varphi)}{R + 2/n} \right], \tag{27}$$

with $\Theta_a = \nu_a \tau$. In this expression the dominant terms will be the ones for which $R \simeq 2/n$, characterizing the resonances. Near a resonance n, equation (27) is then approximated

$$\begin{aligned} J_a &\simeq \frac{m^2 K_n(\mu)}{2\pi n \tilde{\nu}_\varphi} \left[\frac{\cos(2\pi n\Theta_a - 4\pi\Theta_\varphi)}{R - 2/n} \right], \\ \Theta_a &= \nu_a \tau; \end{aligned} \tag{28}$$

in the same approximation,

$$\begin{aligned} J_\varphi &\simeq \frac{m^2 \tilde{K}_n(\mu)}{2\pi n \tilde{\nu}_\varphi} \left[\frac{\cos(2\pi n\Theta_a - 4\pi\Theta_\varphi)}{R - 2/n} \right], \\ \Theta_\varphi &\simeq \tilde{\nu}_\varphi \tau. \end{aligned} \tag{29}$$

The expression

$$R = \frac{\nu_a}{\tilde{\nu}_\varphi} = \frac{2}{n}, \qquad n \geq 2, \tag{30}$$

will determine a curve in the parameter space (E_0, m) where the dynamics is n-resonant. For values of E_0 compatible with initially bounded orbits, the condition $n \geq 2$, is such that the mass m be real.

We are now ready to construct the resonance chart for this model. The expression (30)—where approximations as well as the neglect of non-resonant terms were used—furnish us with lines in the parameter space which constitute an accurate guide for localizing and labelling the actual resonances (see footnote 6). However, in the actual resonant chart constructed numerically using the exact dynamics, the lines will have a spread that is a correction of the approximations due to the full dynamics. Figure 1 is an illustration of the resonant chart for values of $\Lambda = 3/2$ and $Q_0 = 0.01$. These values will be adopted in all the numerical experiments in the paper. The chart of figure 1 corresponds to initial conditions taken near the invariant plane, with $p_a = p_\varphi = 0$, $\varphi = 0.01$. The

JCAP02(2006)015

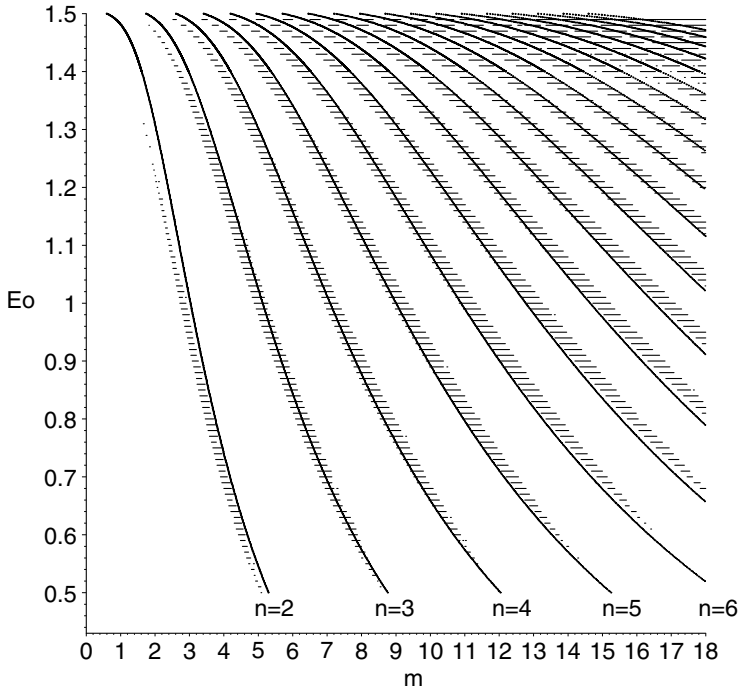

Figure 2. Resonance chart of system (12). The continuous lines are solutions of the approximate resonance condition (30) for $n \geq 2$, while the dark sheets spreading about the lines are regions of disruptive resonances of the exact dynamics (see text).

continuous lines depict the equation $R = \nu_a/\tilde{\nu}_\varphi = 2/n$, $n \geq 2$, while the small sheets spreading about the continuous lines are regions of disruptive resonance of the exact dynamics. In constructing the chart we adopted the value $\tau \simeq 2000$ as an upper limit for testing the instability of the metastable configurations. The remaining regions of the plane correspond to otherwise stable motion. Several numerical tests were made for other initial conditions sufficiently near the invariant plane, and the resonance chart of figure 2 remains accurate to localize instability zones. However, for initial conditions far away from the invariant plane the instability zones tend to spread, and even overlap for values of $m > 0$. This will explain the chaotic sea and secondary islands in regions of the phase space away from the invariant plane, in the maps of section 4 corresponding to m in the zone of parametric stability.

In the remainder of the paper we will approach the problem through the numerical examination of the structure of the full dynamics near a given resonance and between two successive ones.

The basic pattern that emerges immediately after the system passes a resonance window is a characteristic structure of stable periodic orbits, associated with the particular resonance n. These periodic orbits are enclosed by KAM tori and the primary island of KAM dynamics has a border beyond which the dynamics is stochastic filling of large domains of phase space. This is the general picture, but some remarkable differences appear whether the resonance is odd or even, namely $n =$ odd or even, as we proceed to discuss.

3. Schematic analysis of the dynamical pattern near the resonances

We now examine the dynamical pattern associated with the resonances of the model, supported not only by the analytical approximations of the previous section but by also relying on numerical work. All the Poincaré maps discussed in this section and in the remainder of the paper are one-directional; for instance, the map in the surface of section $\varphi = 0$ is made using the standard constraint $p_\varphi \leq 0$ on the surface.

Let us consider an even resonance $n = 2k$. The analytical expressions (28) give us an approximation for (J_a, Θ_a) near the resonance. Since $n = 2k$ we have for this resonance that $T_\varphi = T_a/k$. Let us note that the surface of section $\varphi = 0$ will be crossed at each T_φ. Therefore in the surface of section $\varphi = 0$ of the Poincaré map the variables (a, p_a)—that are one-to-one functions of (J_a, Θ_a)—will take the same value after k crossings of the section. Thus equations (28) and (29) define a periodic orbit with period approximately kT_φ which is characteristic of the particular resonance $n = 2k$. Consequently in the corresponding Poincaré map the periodic orbit will be described by k points. Note that expressions (28) are approximate and were obtained neglecting non-resonant contributions; the full dynamics in a neighbourhood of the characteristic periodic orbit due to these contributions will correspond therefore to $n/2$ primary KAM islands about the stable periodic orbit in the Poincaré section.

Analogously we can obtain from expressions (29) the structure of the Poincaré maps with a surface of section $p_a = 0$ projected in the (φ, p_φ) plane. Indeed for a resonance n we have that $T_a = (n/2)T_\varphi$. Since the points of the Poincaré map for the surface of section $p_a = 0$ are taken at each period T_a it then follows that for even n the Poincaré map will present *one* KAM island while for odd n the number of islands in the map is *two*. In this sense the Poincaré maps with a surface of section $\varphi = 0$ render straightforwardly the order of the resonance while the Poincaré maps with a surface of section $p_a = 0$ inform only if the resonance is even or odd. In the case of even resonances, the above periodic orbit has a companion generated with initial conditions obtained from the previous one by the change $\varphi_0 \to -\varphi_0$. On the contrary, as we will see, odd resonances have only *one* characteristic periodic orbit.

The resonances with integer $n =$ odd have an analogous structure but are, in a certain sense, simpler, having only *one* stable periodic orbit characteristic of the resonance. The analysis of the characteristic periodic orbit connected to an odd resonance and the associated number of primary islands can also be obtained from the approximated analytical expressions (28) and (29). For an odd resonance $n = 2k + 1$ we have that $T_\varphi = (2/2k + 1)T_a$. Thus in the Poincaré surface of section $\varphi = 0$ (that is intersected at each period T_φ) the variables (a, p_a)—which are one-to-one functions of (J_a, Θ_a)—will take the same values only after $(2k + 1)T_\varphi$, corresponding therefore to $2k + 1$ *cuts* in the Poincaré section. Hence a $n = (2k + 1)$ resonance will have an associated characteristic periodic orbit of period $(2k + 1)T_\varphi$, with $(2k + 1)$ primary KAM islands about it. The associated Poincaré map with surface of section $p_a = 0$ presents two islands. It is not difficult to verify numerically that the symmetry transformation of the initial condition of the periodic orbit, $\varphi_0 \to -\varphi_0$, reproduces the same orbit, contrary to the case of $n =$ even. In both cases the periodic orbits are obviously stable. In section 4 we analyse the emergence of characteristic periodic orbits as due to the bifurcation of the stable periodic orbit at the origin $(\varphi = 0, p_\varphi = 0)$ set up by the resonance. The stable periodic orbit at the origin turns unstable through the bifurcation.

Table 1. Classification of resonances according to characteristic periodic orbits.

Resonance	Characteristic periodic orbits	Primary KAM islands, section $\varphi = 0$	Primary KAM islands, section $p_a = 0$
$n = 2k$	2	k	1
$n = 2k + 1$	1	$2k + 1$	2

We summarize the above results in table 1:

In table 1, for even resonances $n = 2k$, the number k of primary KAM islands in the surface of section $\varphi = 0$ refers to each periodic orbit. These results, derived from the approximated analytical expressions (27)–(30), are illustrated in figure 3 constructed with the exact dynamics. There we also exhibit islands of stability in the Poincaré maps with surface of section $\varphi = 0$ and $p_a = 0$, about periodic orbits of the resonance $n = 2$. We have fixed $E_0 = 0.8$, and taken the values $m = 3.800\,85$ slightly beyond the right border (see the chart of figure 2) of the instability zones of the resonance $n = 2$. The presence of the blurred layer in the border of the islands will be the subject of section 5. The maps were constructed with orbits having initial conditions $p_a = p_\varphi = 0$, and $\varphi \geq 0$ for $n = 2$; a more complete extension will given in the next two sections. Main islands about the second characteristic periodic orbit of the resonance would be obtained by the symmetry $\varphi \to -\varphi$.

4. Parametric bifurcation of periodic orbits in the n resonances

As became clear in the previous section, for values of m far from the resonances, the primary KAM island in the Poincaré map with a surface of section $p_a = 0$ encloses the centre (elliptic critical point) $\varphi = 0, p_\varphi = 0$ connected to a stable periodic orbit in the sector (a, p_a). However, as the system crosses a given n resonance, either even or odd, this stable periodic orbit bifurcates into a unstable periodic orbit accompanied by two (for even resonances) or one (for odd resonances) stable periodic orbits. Therefore in the maps the centre at the origin turns into a saddle (hyperbolic critical point), with two centres symmetrically located with respect to it. For even resonances each of the two centres corresponds to one of the two characteristic periodic orbits of the resonance, while for odd resonances the two centres (corresponding to an elliptic point of period $2T_a$) are the section of the single characteristic periodic orbit of the resonance.

The diagram (m, φ_0) of the bifurcation route is given in figure 4 for the resonances $n = 2$, 3 and 4. The value of $E_0 = 0.8$ is fixed. φ_0 denotes the critical points of the map (together with $p_\varphi = 0$) associated with the periodic orbit. We distinguish three types of regions in m. The shaded regions correspond to the range of m where the resonances are disruptive, connected to the dark sheets of the resonance chart of figure 1. Immediately to the left of the disruptive regions, the values of m are such that the origin $\varphi = 0, p_\varphi = 0$ (marked as white dots) is an elliptic point (stable periodic orbit) at the centre of the main KAM island of the map. Continuing to the left, for decreasing values of m towards the resonance n, we reach a third range of m where the elliptic point at the origin bifurcates. The stable and unstable branches of the diagram in this region are shown by white and black dots, respectively. This region is the parametric domain of the resonance n, bounded

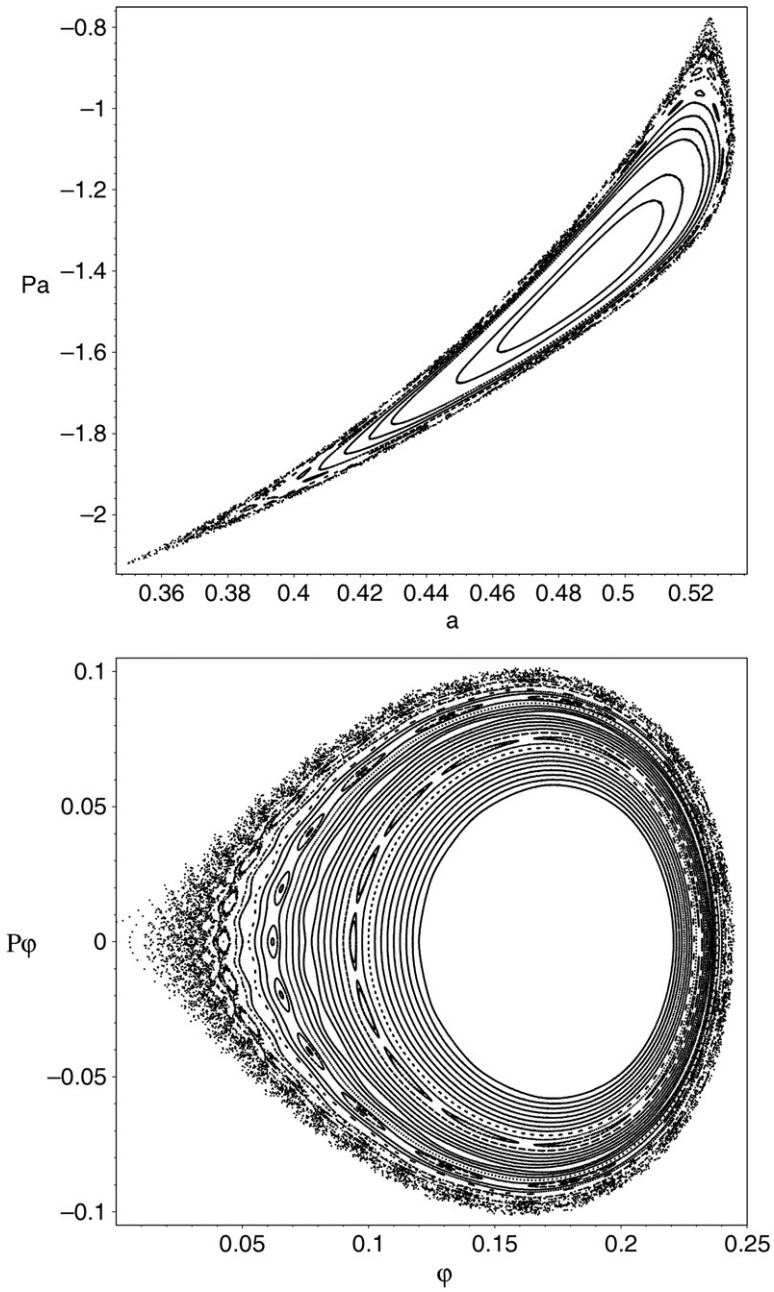

Figure 3. Poincaré maps with surface of section $\varphi = 0$ (top) and $p_a = 0$ (bottom), for the value $m = 3.800\,85$ in the parametric region of resonance $n = 2$. The maps show the main islands about the periodic orbit corresponding to the centre ($\varphi_0 \approx 0.18, p_{\varphi_0} = 0$), and for times $\tau \leq 4000$.

on the left by the dark disruptive region of n. We remark that, for odd resonances, the white dots related by $\varphi_0 \to -\varphi_0$ in the parametric domain of the resonance are period-two fixed points connected to the single periodic orbit of the resonance (see table 1 of section 3). The crossing of a resonance n is meant to pass from the left (stability domain) to the right (bifurcated domain) of the shaded area.

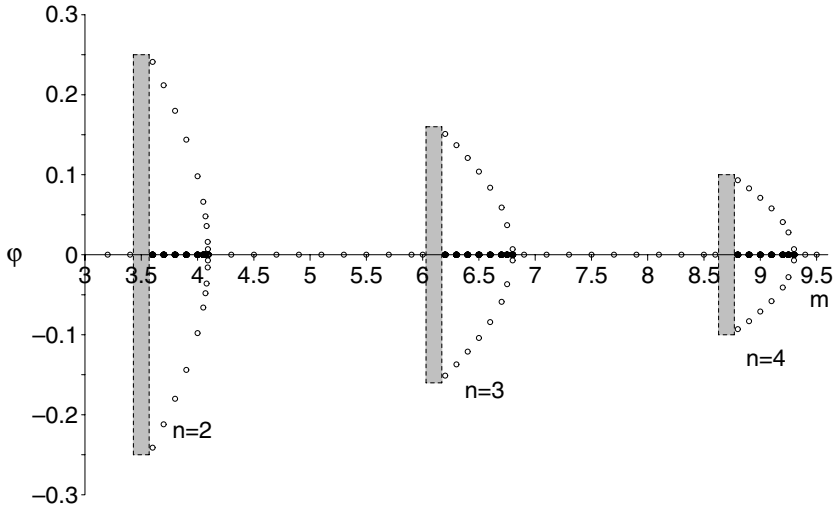

Figure 4. Diagram (m, φ_0) of parametric bifurcation of the periodic orbit at the origin $(\varphi = 0, p_\varphi = 0)$, between the resonances $n = 2$ and $n = 4$. The shaded regions correspond to values of m connected to disruptive resonances for initial condition values near the invariant plane $(\varphi = 0, p_\varphi = 0)$. On their left is the region of parametric stability for the periodic orbit. Further to the left, a value of m is reached beyond which the periodic orbit at the origin bifurcates. The stable and unstable branches are shown by white and black dots, respectively, marking the parametric domain of the resonance.

We are now ready to compare the dynamical behaviour of the system in the parametric domain of a n resonance as opposed to the behaviour in the region of parametric stability. We will consider the value of $m = 3.800\,85$ corresponding to the parametric domain of the resonance $n = 2$ and $m = 4.29$ corresponding to the region of parameter stability between the resonances $n = 2$ and $n = 3$. The latter value was fixed according to the diagram of figure 4. Poincaré maps with a surface of section $p_a = 0$ are used for comparison purposes, since they have a close analogy with the standard map that was extensively studied in connection with the existence of Cantori and diffusion of orbits in [16][7]–[20] and will be a guide to the discussion of the next section. In the map corresponding to $m = 3.800\,85$, shown in figure 5 (top), the two main islands are centred about $(\varphi_0 \simeq \pm 0.18, p_{\varphi_0} = 0)$ and the origin is a hyperbolic point. Beyond the border of the main islands, we note the large region of phase space corresponding to long-time diffusion (before the orbits escape to inflation). The stochastic sea beyond the fuzzy border of the main islands presents the structure of a web through which diffusion takes place to large regions of phase space, being due to the horseshoe [16] structure of the crossing of the separatrices connected to the saddle at the origin. No islands are seen in this region. The characteristics of diffusion mentioned so far and in the remainder of the section will be discussed in section 5. This is opposed to the Poincaré map for $m = 4.29$ in the region of parametric stability,

[7] For a clear and concise introduction to the standard map, including the occurrence of Cantori and transport theory connected to them, and packages for numerical simulations, see Meiss's pages:
http://amath.colorado.edu/faculty/jdm/index.html and
http://www.me.ucsb.edu/course_pages/course_pages_f05/me201/reading.html.

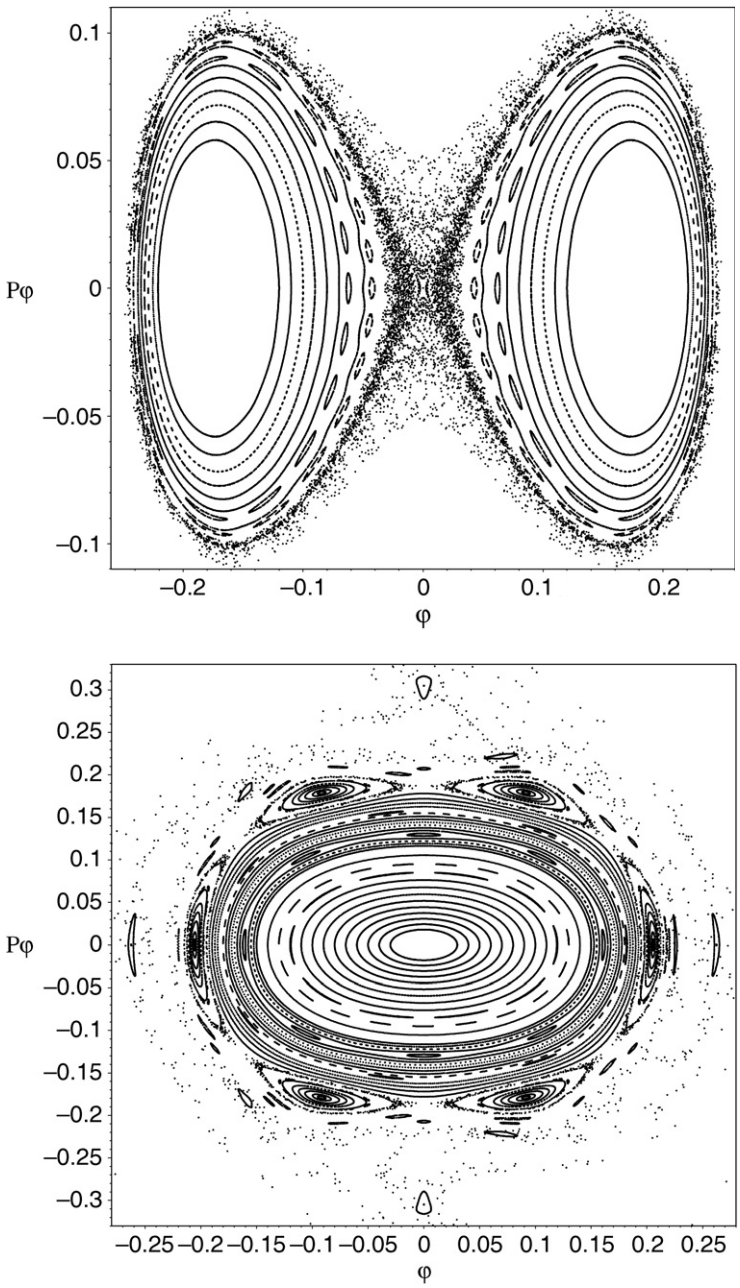

Figure 5. Poincaré maps with a surface of section $p_a = 0$ for $m = 3.800\,85$ in the domain of parametric resonance $n = 2$ (top), and $m = 4.29$ in the domain of parametric stability between the resonances $n = 2$ and $n = 3$ (bottom). The origin in the first map (top) is a saddle with two associated centres, a consequence of the bifurcation of the periodic orbit due to the resonance $n = 2$. The structure of the stochastic sea differs in each case (see text). The maps were constructed with $\tau = 4000$.

where the main island is centred about the origin and the stochastic sea beyond the border of the main island contains several secondary islands. The diffusion of orbits (with initial conditions beyond the border of the main island) in the stochastic sea towards the de Sitter infinity is extremely rapid. The map is displayed in figure 5 (bottom), where we have considered initial conditions $p_\varphi = 0 = p_a$, with $\varphi \geq 0$ only to avoid overcluttering the figure. For instance, the sets of 5, 6, 11 and 16 secondary islands seen in the stochastic sea enclose periodic orbits with $R = \nu_a/\nu_\varphi = 5/6,\ 6/7,\ 11/13,\ 16/19$ (since the corresponding map with a surface of section $\varphi = 0$ presents 6, 7, 13 and 19 secondary islands, respectively). A further set of 5 and 11 secondary islands symmetrical to the previous ones would show up if we had included in the generation of the map initial conditions with $\varphi \leq 0$.

The crucial point for the dynamics of inflation is the instability versus the stability of the origin $\varphi = 0,\ p_\varphi = 0$. The differences in the two situations will have a bearing on the dynamics of the spatially homogeneous expectation values $\varphi(\tau)$ of the inflaton field related to the escape into inflation. Let us recall that the energy momentum tensor of the inflaton may be split into a cosmological constant-type term (corresponding to the vacuum energy of the inflaton field) plus the energy momentum tensor of the spatially homogeneous expectation values of the inflaton field. In this instance the initial conditions of the expectation values φ are assumed to be small, and are to be taken near the invariant plane $\varphi = 0,\ p_\varphi = 0$, that corresponds to a neighbourhood of the critical point of the map at the origin $(\varphi = 0, p_\varphi = 0)$. Therefore the region of parametric stability of the system will be unfavourable for the physics of inflation since the orbit (a configuration of the early universe) will be trapped in a stable state between two KAM tori near the centre of the main island. However, if the system is in the region of parametric resonance, initial conditions near the invariant plane would undergo a long-time diffusion through stochastic webs to large regions of phase space, and finally escape to the de Sitter asymptotic configuration at infinity. Another difference lies in the fact that when the system is in the region of parametric stability initial conditions for orbits that diffuse are far from the invariant plane, and diffusion with escape to de Sitter infinity is extremely rapid. The characteristics of diffusion mentioned so far will now be discussed.

A final remark is in order here. Since the definition of the domain of either parametric resonance or parametric stability depends on (E_0, m, φ_0), where φ_0 is associated with the initial condition of the inflaton, resonance phenomena may also be present for values of $m < 1$ and $\varphi_0 > 1$. For instance, in the parametric domain about $E_0 = 0.8$, $m = 0.22$ and initial condition $\varphi = 1.16$ ($p_a = 0 = p_\varphi$ as always) a resonance $n = 2$ is present (equivalently $R = 1$), corresponding to one secondary island in the surface of section $p_\varphi = 0$ and one associated secondary island in the surface of section $p_a = 0$. The dynamics of this resonant domain is localized in the stochastic sea about a primary island enclosing the origin $(\varphi = 0, p_\varphi = 0)$, in a configuration analogous to figure 5 (bottom). A more detailed analysis of these resonances for initial configurations away from the invariant plane and $m < 1$ will be the subject of future work.

5. Diffusion and Cantori

Let us consider the case of resonance $n = 2$. In the island of stability of figure 3 (top) for the surface of section $\varphi = 0$, the orbits are either on a KAM torus or contained

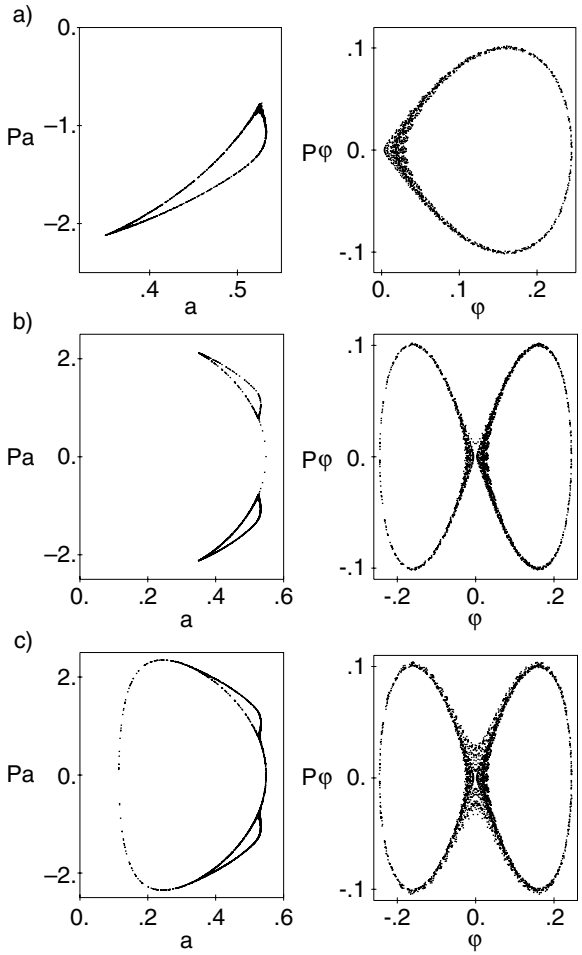

Figure 6. Poincaré maps for one orbit with initial conditions in the border of the main island of the resonance $n = 2$. (a) Map of the orbit up to $\tau \simeq 4540$ (corresponding to 1245 iterations in the map (a, p_a)). (b) Beyond 1245 iterations the orbit is seen to undergo a diffusion escaping from the neighbourhood of the original section and enclosing the island about the second characteristic periodic orbit of the resonance. This is evidence of the presence of a Cantorus in the border of the main islands. (c) For later times, $\tau \simeq 7440$ (or 1520 iterations of the map), the orbit undergoes complete diffusion (see also figure 7).

between two sufficiently close KAM tori. As we explore more extended regions of phase space far from the periodic orbit we reach the border of the island which appears in the figure as an ill-defined thin dark layer. We still maintain the value of $m = 3.800\,85$ in the same energy surface $E_0 = 0.8$ but now we evolve an orbit with the initial condition $(p_\varphi = p_a = 0, \varphi = 0.010\,010\,001, a = 0.114\,640\,667\,0921\,826)$ taken in the border of the main island. The motion of the orbit is displayed in figures 6, through the Poincaré map with a surface of section $\varphi = 0$ for several distinct times. Figure 6(a) shows the map of the orbit up to $\tau = 4540$, corresponding to 1245 iterations in the map with a surface of section $\varphi = 0$. It is seen to enclose the main island of figure 2(a), meaning that up to this time the motion of the orbit takes place in a narrow finite portion of phase space (one *lobe*

in the border of the main island). Beyond 1245 iterations we see from figure 6(b) that the orbit undergoes a diffusion escaping from the neighbourhood of the original section and enclosing the island about the second characteristic periodic orbit of the resonance. This is evidence that this orbit was initially enclosed between a KAM torus and a Cantorus, or between two Cantori, in the *lobe* and that after 1245 iterations it encountered a hole (gap) in the external Cantorus and escaped to a larger region of phase space. Finally in figure 6(c) for times $\tau > 7440$ (equivalently, after 1520 iterations), the orbit undergoes complete diffusion. This orbit is one of the stochastic seas in the map of figure 5 (top).

The presence of Cantori in the border between stability islands and the stochastic sea, and their dynamics, has been widely discussed in the literature mainly for the case of the standard map (see [16]–[20], footnote 7 and the two paragraphs below). The Poincaré maps of our system with a surface of section $p_a = 0$ given in the variables (φ, p_φ) have a close analogy with the standard map (especially those in the parametric stability region, see figure 5 (bottom)) so that the results of the above references can indeed be used here as a basic analysis of the dynamical phenomena that occur with orbits in the border, and their diffusion. For the benefit of readers we introduce briefly some basic notions related to Cantori and give relevant references that we consider allow for a more complete understanding of the subject.

Cantori are basically the remnants of KAM tori that are destroyed if either the nonlinear perturbation is increased or the control parameters of the system, namely (E_0, m) in our system, are suitably varied. As a matter of fact, as the parameters are varied, Cantori can be created or destroyed or change their structure. The surface of section of a Cantorus is an invariant Cantor set of points under the dynamics, and corresponds to a quasi-periodic orbit that has the rotation number of the KAM torus destroyed. The image of a Cantorus may be that of a torus full of holes [16]. Cantori may allow a small flux of orbits through them and a theory of diffusion in Hamiltonian systems connected to the presence of Cantori has been the subject of much recent interest [17]. Cantori are usually located at the border between main islands, or between chains of secondary islands and the stochastic sea of the dynamics. Their existence was proposed by Percival and Aubry [18], who gave an explicit example connected to the dynamics of the standard map. A general proof of their existence was given by Aubry and Le Daeron, Mather and Katok [19].

Orbits initially in a region bounded by two KAM tori cannot cross the bounding KAM tori into the other regions of phase space. By increasing the nonlinearity parameter, bounding KAM tori break and turn into a Cantorus making it possible for chaotic orbits to diffuse into the large stochastic sea through the holes in the Cantorus. Cantori constitute partial barriers to the diffusion of orbits in the stochastic sea and the motion may be trapped for a long time between two Cantori before leakage through their gaps [17]. In the numerical analysis of a system's diffusion within a stochastic region, the Cantori manifest themselves as follows. First the random motion takes place in a narrow finite portion of phase space (motion is caught in a certain layer, between a KAM torus and a Cantorus or between two Cantori). Further, the trajectory breaks through an invisible Cantorus quickly filling a far greater portion of phase space. Now the motion is limited by another Cantorus and continues until a next breakthrough occurs, and the numerical figures depict only the most conspicuous breakthroughs among them. For instance, in the case of large K in the standard map, the Cantori are very 'porous' and the effective length

of the barriers becomes extremely small [20]. We may note that Cantori are present not only in the border of primary islands but also in those of of higher-order secondary islands. For instance in the map of figure 5 (bottom) we can note that the 6/7 secondary islands are detached from the main island, and we can verify numerically that orbits with initial conditions in its border will diffuse around them for a very long period, in a behaviour analogous to that of figure 6, before entering the chaotic sea when it escapes to de Sitter rapidly. Furthermore through numerical experiments we have evidence of the presence of Cantori enclosing the 5/6, 6/7, 11/13 and 16/19 islands. Escape from this region takes place after at least 10^5 iterations.

However, the diffusion when the system is in the zone of parametric resonance has some striking differences from the previous case. Due to the bifurcation of the centre at the origin into a saddle (see figure 5 (top)) and due to the non-integrability, the stochastic sea beyond the smeared out border of the main islands presents the structure of a web through which diffusion takes place to large regions of phase space. The origin of the stochastic web is due to the horseshoe structure originating from the breaking and infinitely many crossings of the separatrices emerging from the saddle at the origin [16]. No islands are seen in this region. This will indeed be the typical pattern of the dynamics of spatially homogeneous averaged fluctuations of the inflaton as the system evolves to an inflationary phase. On the contrary, as already discussed, in the parametric stability region these fluctuations are trapped between KAM tori and the system is unable to enter the inflationary phase. In both cases we note that whenever the orbit diffuses into the stochastic sea its motion is random and it always escapes to the de Sitter infinity.

In figure 7 we display the web pattern formed in the map corresponding to the orbit of figure 6, for a very long time and enlarged about the saddle at the origin, due to the resonance $n = 2$. This long-time process of diffusion ends up in the escape of the orbit to the de Sitter infinity (escape to inflation).

The diffusion in the case of odd resonances is basically analogous, with the distinction that the three lobes are already formed before the diffusion of orbits through a Cantorus takes place. This is connected to the fact that odd resonances have only one characteristic periodic orbit.

A careful observation of the time development of the Poincaré section for the surface of section $\varphi = 0$ projected in (a, p_a) shows that it develops as if, in later stages, the orbit had three basic attracting neighbourhoods, the first two developed about the two symmetric characteristic periodic orbits of the resonance (corresponding to the symmetry $\varphi \to -\varphi$) and the third one connected to the remnant tori of the stability region in the parameter space. The diffusion from one attracting neighbourhood to another is made through the stochastic web connected to the separatrices of the saddle point at the origin. For the regime of fully established diffusion, an examination of the function $\varphi(\tau)$ shows that the time duration in which the orbit remains in one of the attracting neighbourhoods, as well as the next one to be attained, is completely random. The analysis of the time signal $\varphi(\tau)$ will be the object of future work, the motivation of which for the physics of inflation is discussed in the conclusions.

6. Final discussions and conclusions

In this paper we have examined the dynamics of positively curved inflationary models in which quantum gravity corrections to General Relativity are considered, leading to

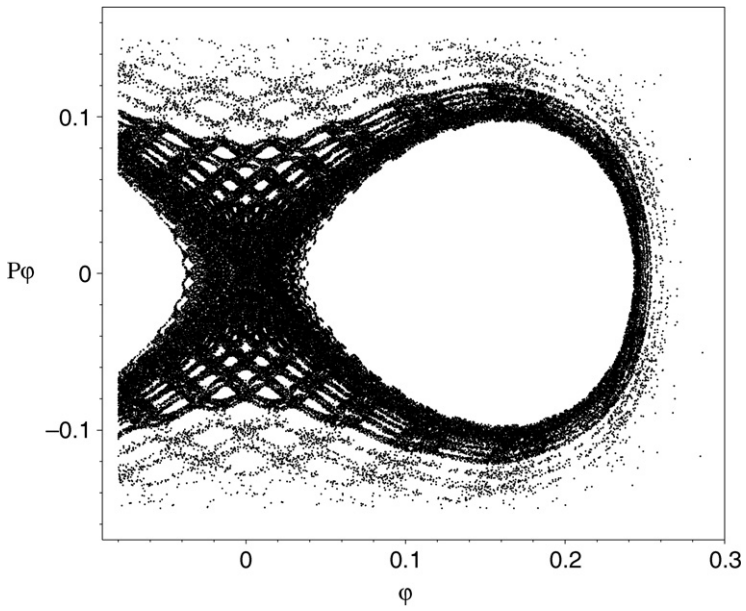

Figure 7. The stochastic web pattern formed in the map with a surface of section $p_a = 0$ for the orbit of figure 6, and enlarged about the saddle at the origin. The map was computed for a very long time, until the escape of the orbit to the de Sitter infinity.

the presence of non-singular bounces in the scale factor of the models. The form of these corrections is derived from brane-world models and result in a repulsive force that avoids the singularity and provides a concrete model for bounces in the early phase of the universe. These effects will be dominant in regions of high curvature and create metastable configurations for the universe, corresponding to dynamical orbits confined between KAM tori or between a KAM torus and a Cantorus. The dynamics is non-integrable and chaotic if the mass of the inflaton $m \neq 0$.

For certain windows of the parameter space (E_0, m) of the model nonlinear resonance of KAM tori is set up, with a complex dynamics that involves the diffusion of orbits through Cantori into a stochastic sea. Each resonance is characterized by an integer $n \geq 2$ and its main feature is the bifurcation of the stable periodic orbit at the origin $(\varphi = 0, p_\varphi = 0)$ into an unstable periodic orbit accompanied by one or two characteristic stable periodic orbits depending on whether n is odd or even, respectively. This characterizes the parametric domain of the n resonance (see figure 4). Since the initial conditions of the expectation values φ are assumed to be small and are then taken near the invariant plane $\varphi = 0$, $p_\varphi = 0$, it follows that the parametric domain of resonance is the one that strongly favours inflation in the system. Actually at this domain of parameters initial conditions near the invariant plane belong to a neighbourhood of the saddle at the origin $(\varphi = 0, p_\varphi = 0)$ of the map with a surface of section $p_a = 0$ (see figure 5 (top)) and the associated orbits have a long-time diffusion into the large stochastic sea. Diffusion ends up with the escape of the orbits to the de Sitter infinity, corresponding to the universe entering the inflationary phase. On the contrary, in the region of parametric stability the orbits will be trapped in a stable state between two KAM tori near the centre

JCAP02(2006)015

at the origin ($\varphi = 0, p_\varphi = 0$) (see figure 5 (bottom)) and inflation is not favoured; initial conditions that diffuse in this case are far from the invariant plane, and the diffusion is extremely rapid.

The above phenomena are generic for closed inflationary models, as long as bounces are included in the theory. In fact, the minimal ingredients in the inflationary paradigm [21] are a FRW geometry plus a scalar field, the inflaton field, together with well-formulated ideas of modern quantum field theory. The basic idea of inflation is that the vacuum energy of the inflaton field was the dominant component of the energy density of the universe in an early epoch of its evolution. The dynamics, ruled by Einstein's equations, has thus a cosmological constant-type term (connected to the vacuum energy of the inflaton field) and the two degrees of freedom $a(\tau)$ and $\varphi(\tau)$, respectively the scale factor and the spatially homogeneous expectation value of the inflaton field. In general the resulting potential for φ always has a minimum, thus providing the condition for nonlinear resonance.

In the domain of parametric resonance, the time period in which a diffused orbit remains in the neighbourhood of one of the *lobes* about main islands is completely random. The passage from one *lobe* to another is made through the stochastic web set up in the dynamics by the resonance. This phenomenon is in the realm of a diffusion-transport theory in Hamiltonian systems connected to the presence of partial barriers to the diffusion of orbits into the stochastic sea, created by Cantori, and has been the object of much recent research [17]. A signature of this randomness may be obtained if we make a frequency analysis of the time signal of one of the variables, let us say $\varphi(\tau)$, associated with a long-time diffusion orbit (see for instance figure 6) before escaping into inflation. In the frequency spectrum we can verify the presence of a group of very low frequencies above a broad background. If by a filtering procedure we reconstruct the time signal with just this group of low frequencies, it results in large-scale intermittency; analogously a group of higher frequencies above the background is present and the reconstruction of the time signal with just these frequencies yields intermittency at smaller scales. This is characteristic of a turbulent regime that might lead to thermal fluctuations and could provide an alternative mechanism for the origin of cosmic structure, as has been recently suggested [22]. On the other hand, some dominant frequencies are present in the spectrum, multiples of the frequencies of the characteristic periodic orbits of the resonance. Enhancement of perturbations with wavenumbers corresponding to these dominant characteristic frequencies is also expected. We will come to these issues in a future publication.

Finally, if the above processes actually occurred in the early dynamics of the universe, the spectrum of perturbations should then have a signature of the particular resonance and consequently of the particular value of the mass parameter of the inflaton that was favoured in the early dynamical regime of the universe.

Acknowledgments

We thank Professor A M Ozorio de Almeida for comments on the manuscript. The authors also acknowledge partial financial support from CNPQ/Brasil. Many of the figures were generated using the *Dynamics Solver* packet [23].

References

[1] Bojowald M, 2001 *Phys. Rev. Lett.* **86** 5227 [SPIRES]
Singh P and Toporensky A A, 2004 *Phys. Rev.* D **69** 104008 [SPIRES]

[2] Koury J *et al*, 2002 *Phys. Rev.* D **65** 086007 [SPIRES]
Tsujikawa S, Brandenberg R and Finelli F, 2002 *Phys. Rev.* D **66** 083513 [SPIRES]
Gasperini M, Giovannini M and Veneziano G, 2002 *Phys. Lett.* B **569** 113 [SPIRES]
Fabris J C *et al*, 2003 *Phys. Rev.* D **67** 124003 [SPIRES]
Basset B *et al*, 2003 *Phys. Rev.* D **67** 123506 [SPIRES]
Koury J, Steinhardt P J and Turok N, 2004 *Phys. Rev. Lett.* **92** 031302 [SPIRES]

[3] Belinskii V A, Grishchuk L P, Zeldovich Ya B and Khalatnikov I M, 1985 *Sov. Phys. JETP* **62** 195 [SPIRES]
Parker L and Fulling S A, 1973 *Phys. Rev.* D **7** 2357 [SPIRES]
Starobinski A A, 1978 *Sov. Astron. Lett.* **4** 82

[4] Hawking S W, *Relativity, groups and topology II*, 1984 *Proc. Les Houches Summer School (June–Aug. 1983)* ed B S DeWitt and R Stora (London: Gordon and Breach)
Page D, 1984 *Class. Quantum Grav.* **1** 417 [SPIRES]
de Oliveira H P and Damião Soares I, 1999 *Phys. Rev.* D **60** 023512 [SPIRES]
Kamenshchik A Yu, Khalatnikov I M and Toporensky A V, 1997 *Int. J. Mod. Phys.* D **6** 673 [SPIRES]

[5] Peter P and Pinto-Neto N, 2002 *Phys. Rev.* D **66** 063509 [SPIRES]

[6] Campos A and Sopuerta C F, 2001 *Phys. Rev.* D **63** 104012 [SPIRES]
Shtanov Y and Sahni V, 2003 *Phys. Lett.* B **557** 1 [SPIRES]
Lidsey J E, Mulryne D J, Nunes N J and Tavakol R, 2004 *Phys. Rev.* D **70** 063521 [SPIRES]

[7] Peter P and Pinto-Neto N, 2002 *Phys. Rev.* D **66** 0635509 [SPIRES]
For negative values of A see Khalatnikov I M and Kamenschchik A Yu, 2003 *Phys. Lett.* B **553** 119 [SPIRES]

[8] Faraoni V, 2000 *Phys. Rev.* D **62** 023504 [SPIRES]
Faraoni V, 2001 *Int. J. Theor. Phys.* **40** 2259 [SPIRES]

[9] Birrell N D and Davies P C, 1982 *Quantum Fields in Curved Space* (Cambridge: Cambridge University Press)

[10] Lachièze-Rey M and Luminet J P, 1995 *Phys. Rep.* **254** 135 [SPIRES]
Fagundes H, 1989 *Astrophys. J.* **338** 618 [SPIRES]

[11] Mielke A, Holmes P and O'Reilly O, 1992 *J. Dyn. Differ. Eqns* **4** 95
Hirsch M W, Smale S and Devaney R L, 2004 *Differential Equations, Dynamical Systems & An Introduction to Chaos* (New York: Elsevier Academic Press)
Monerat G A, Oliveira H P and Damião Soares I, 1998 *Phys. Rev.* D **58** 063504 [SPIRES]

[12] Abramowitz M and Stegun I, 1964 *Handbook of Mathematical Functions* (*NBS Applied Math. Series* vol 55) (Washington, DC: National Bureau of Standards)

[13] Kolmogorov A N, 1979 *Stochastic Behaviour in Classical and in Quantum Hamiltonian Systems* (*Lecture Notes in Physics* vol 93) ed G Casati and J Ford (Berlin: Springer)
Arnold V I, 1963 *Russ. Math. Surv.* **18** 9
Moser J, 1962 *Nachr. Akad. Wiss. Goett.* IIa **2** 1–20

[14] Guckenheimer J and Holmes P, 1983 *Dynamical Systems and Bifurcations of Vector Fields* (New York: Springer)

[15] Chirikov B V, 1979 *Phys. Rep.* **52** 263 [SPIRES]

[16] Meiss J D, 1992 *Rev. Mod. Phys.* **64** 795 [SPIRES]

[17] Chirikov B V and Shepelyansky D L, 1984 *Physica* D **13** 363
MacKay R S, Meiss J D and Percival I C, 1984 *Physica* D **13** 55
Dana I and Fishman S, 1985 *Physica* D **17** 63
Meiss J D and Ott E, 1986 *Physica* D **20** 387

[18] Percival I C, 1979 *Nonlinear Dynamics and the Beam–Beam Interaction* (*AIP Conf. Proc.* vol 57) ed M Month and J C Herrera, New York p 302
Percival I C, *Dynamical chaos*, 1987 *Proc. Roy. Soc. Meeting (London, 1987)*
Aubry S, 1978 *Solitons and Condensed Matter Physics* (*Springer Series in Solid-State Sciences* vol 8) ed A R Bishop and T Schneider (New York: Springer)

[19] Aubry S and Le Daeron P Y, 1983 *Physica* D **8** 381
Mather J M, 1982 *Topology* **21** 457

Katok A, 1982 *Ergodic Theory Dyn. Syst.* **2** 185
[20] Zaslavsky G M, Sagdeev R Z, Usikov D A and Chernikov A A, 1991 *Weak Chaos and Quasi Regular Patterns* (Cambridge: Cambridge University Press)
[21] Kolb E W and Turner M S, 1990 *The Early Universe* (New York: Addison-Wesley)
Linde A, 1991 *Particle Physics and Inflationary Cosmology* (Switzerland: Harwood Academic)
[22] Maqueijo J and Pogosian L, 2003 *Phys. Rev.* D **67** 043518 [SPIRES]
[23] Aguirregabiria J M, 2005 Dynamics Solver http://tp.lc.ehu.es/jma.html

JCAP02(2006)015